ELSEVIER

Chemical Engineering Journal 72 (1999) 109–116

Chemical Engineering Journal

Characterization of axial liquid dispersion in gas–liquid and gas–liquid–solid reactors

G. Hebrard*, D. Bastoul, M. Roustan, M.P. Comte, C. Beck

Lipe E.A. 833 Département Génie des Procédés Industriels, Institut National des Sciences Appliquées, 31077 Toulouse, France

Received 20 April 1998; received in revised form 17 October 1998; accepted 26 October 1998

Abstract

Axial liquid mixing was studied in gas–liquid systems (bubble columns) and two types of gas–liquid–solid system (the turbulent and inverse turbulent beds) for different types of gas sparger (membrane and perforated plate). In the turbulent and inverse turbulent beds, solids, larger and lighter than water and of large diameter (3–4 mm) are fluidized only by an upward gas flow. In two-phase systems, the type of gas sparger has a strong effect on the gas flow regime and consequently on the axial liquid mixing. A general diagram with coordinates Pe versus $Fr^{(1/3)}$ has been established in order to explain all the results. It allows the hydrodynamic characteristics to be predicted by a simple measurement of the axial liquid dispersion coefficient E_{zl}. In the gas–liquid–solid reactors tested, the effect of the gas sparger on axial liquid mixing can be pronounced. A flow regime diagram is proposed, which shows a heterogeneous flow behaviour independent of the gas sparger when the solid content of the column is sufficiently high.

Keywords: Bubble column; Turbulent bed; Inverse turbulent bed; Gas sparger; Axial liquid mixing; Dimensionless general diagram

1. Introduction

Axial mixing of the liquid phase in a bubble column (BC) has been extensively investigated. It is generally described by the axial liquid dispersion coefficient E_{zl}. Deckwer et al. [1], Baird and Rice [2], Joshi [3], Rice et al. [4], and Kawase and Moo-Young [5] have measured this liquid axial dispersion coefficient in BCs. All of their results indicate that E_{zl} depends strongly on the superficial gas velocity and the column diameter. However, the influence of the liquid phase properties and the gas sparger are not clearly understood.

In a previous study, we presented results on the influence of the gas sparger on the hydrodynamic behaviour of BCs [6]. Three columns with inner diameters of 0.08, 0.15 and 0.2 m, each 2 m high, were used and three types of gas sparger were studied (perforated plates, porous disc diffuser, flexible rubber spargers). Four gas flow states were identified (Fig. 1), depending on the superficial gas velocity, the column diameter and the type of gas sparger. In addition, it was shown that the intensity of the liquid axial mixing depends strongly on the gas sparger and can be influenced by the gas flow conditions.

We propose that the axial liquid mixing could be characterized by means of two dimensionless numbers, the Peclet and Froude numbers; in the BCs, the ratio $Pe/Fr^{(1/3)}$ can be calculated by the following equation [6];

$$\frac{Pe}{Fr^{(1/3)}} = 2.326\left(\frac{e}{(1-e)}\right)^{(1/3)} \quad (1)$$

with

$$Pe = \frac{U_g D_c}{E_{zl}}, \qquad Fr = \frac{U_g^2}{gD_c}, \qquad e = \frac{U_s}{U_{b_\infty}}$$

where U_{b_∞} is the terminal velocity of rising air bubbles in water at 20°C predicted by Grace [7] and U_s is the slip velocity defined by Wallis [8].

It has been shown by Hébrard et al. [6] that the value of e depends on the gas sparger and can reveal the nature of the gas flow regime: with a membrane disc, e is close to 1, whereas it can reach 1.5 with a perforated plate. Thus, a low value of e can be associated with perfect bubbly flow and a high value of e characterizes imperfect or heterogeneous gas flow.

This may explain the large discrepancy of the results in the literature since the type of gas sparger used is not taken into account. Furthermore, the use of various relationships is

*Corresponding author.

1385-8947/99/$ – see front matter
PII: S1385-8947(98)00151-X

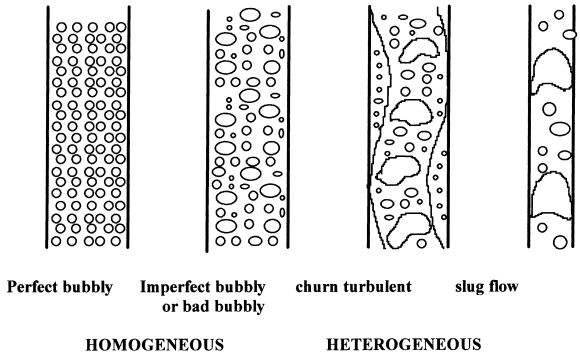

Fig. 1. Gas flow regimes.

often restricted to the operating conditions and to the pilot scale reactor used for their establishment.

With regard to gas–liquid–solid (G–L–S) reactors, extensive work is available on two types of multiphase reactor: the classical three-phase fluidized bed (TPFB) and the slurry bubble column.

Nacef et al. [9] investigated the effect of the gas sparger and of the scale of the column on the minimum fluidization velocity and the flow regime in the TPFB.

Kato et al. [10], used glass beads ($63\ \mu m < d_p < 177\ \mu m$) and characterized the axial liquid mixing in columns 6.6, 12.2 and 21.4 cm in diameter. They reported that the axial liquid dispersion coefficient E_{zl} increases with the gas velocity at low liquid throughput and that the liquid mixing in the TPFB is very similar to that in a BC.

Michelsen and Østergaard [11] and Østergaard [12], showed that with glass beads the intensity of axial liquid mixing depends upon the particle size and superficial gas and liquid velocities.

El-Temtamy et al. [13] and Kim and Kim [14], characterized the axial liquid mixing in TPFBs of 0.05–0.145 m inner diameter, with glass beads of 0.45–6 mm average diameter. They showed that the coefficient E_{zl} increases with increasing particle size and depends on the superficial gas and liquid velocities.

Joshi [3] proposed the following relations for E_{zl}, applicable to BCs and TPFBs

$$E_{zl} = 0.33(V_c + U_l)D_c \qquad \text{(BC)} \tag{2}$$

and

$$E_{zl} = 0.29(V_c + U_l)D_c \qquad \text{(TPFB)} \tag{3}$$

where V_c is the circulation velocity calculated from the energy balance method on the basis of Whalley and Davidson's [15] approach

$$V_c = 1.31\left\{gD_c\left[U_g - \varepsilon_g U_{b_\infty}\right]\right\}^{(1/3)} \qquad \text{(BC)} \tag{4}$$

$$V_c = 1.31\left\{gD_c\left[U_g + U_l - \frac{\rho_l U_l}{\varepsilon_s\rho_s + \varepsilon_l\rho_l} - \varepsilon_s\left(\frac{\rho_s}{\varepsilon_s\rho_s + \varepsilon_l\rho_l} - 1\right)V_s - \varepsilon_g U_{b_\infty}\right]\right\}^{1/3} \qquad \text{(TPFB)} \tag{5}$$

When the weight of solids in the column and/or V_s are low, Eq. (5) reverts to Eq. (4) available for gas–liquid (G–L) systems.

However, although extensive work has been performed on these hydrodynamic parameters in G–L systems and classical TPFBs using heavy particles, there is little information on TPFBs using large or light particles. Furthermore, hardly any information is available on multiphase reactors, such as the turbulent bed or the inverse turbulent bed. In these three-phase systems the particles whose density remains quite close to the density of water ($\pm$20–40 kg/m^{-3}) are fluidized by the upward gas flow only; the liquid flow, when used, is too slow to move the particles.

In the same way, the influence of the weight of solids introduced in the reactor on the liquid mixing is rarely mentioned. In addition, as in G–L systems, the influence of the type of gas sparger is not taken into account and the equations do not have a large range of applications. As the liquid mixing is characterized by the single parameter E_{zl}, it is impossible to compare the specificity of one multiphase reactor with other types of multiphase reactor.

The objectives of the present research are as follows:

1. In G–L systems, to propose a general diagram, on the basis of the dimensionless numbers Pe and Fr, predicting the nature of the gas flow regime and the intensity of the axial liquid mixing, whatever the type of G–L contactor.
2. To characterise the axial liquid mixing generated in multiphase reactors such as the turbulent bed [16] and inverse turbulent bed [17].
3. To extend the use of the general diagram proposed in G–L systems to G–L–S systems.

2. Experimental details

A schematic diagram of the experimental apparatus is shown in Fig. 2(a). Experiments were performed on two columns (1 and 2) of 0.20 and 0.385 m inner diameter and 4 m in height. The principles of the turbulent bed and the inverse turbulent bed are schematically presented in Fig. 2(b) and Fig. 2(c). Three gas spargers, a perforated plate and two flexible membrane discs were used. The sparger characteristics and their connection with the columns are described in Tables 1 and 2. Except for membrane II, the gas sparger covered the whole cross-section of the columns. Water and air were used as the liquid and gas phases, all the experiments being performed with no throughput of liquid. The solid particles were made of polyethylene or polystyrene. In order to exclude the influence of plasticizers, they were made wettable before use. Their physical properties are summarized in Table 3. Experiments were carried out in the two columns by varying the initial weight of solids introduced into the reactor. The different mass of solids used are reported in Table 4. This was characterized by the dimensionless mass number, Ma,

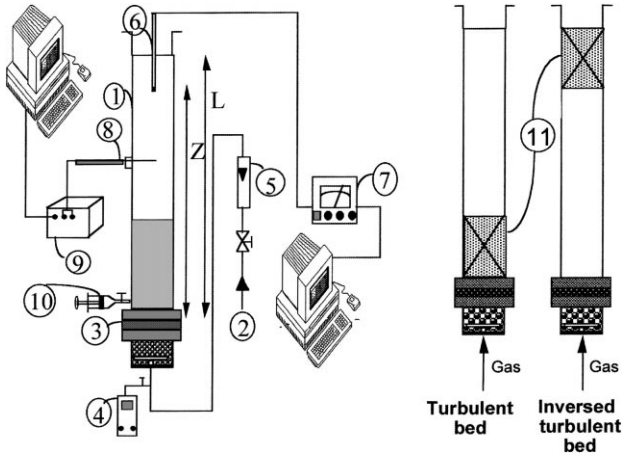

Fig. 2. Diagram of experimental apparatus: 1, column; 2, gas inlet; 3, sparger; 4, electronic Manometer; 5, rotameter; 6, conductivity cell; 7, conductivity bridge; 8, optical probe; 9, optoelectronic module; 10, tracer injection; 11, solid particles.

defined as follows:

$$\mathrm{Ma} = \frac{m_\mathrm{p}}{\rho_\mathrm{s} D_\mathrm{c}^3}$$

where m_p is the mass of solids, ρ_s is the density of particle material and D_c is the column diameter. Mass number was varied between 0 to 5 during the experiments.

Axial mixing was described by the dispersion model. A transient state method was used. A salt tracer pulse (NaCl, 250 g l^{-1}) was added at the bottom of the column just above the gas distributor, and the time variation of the tracer concentration was detected at a height of 3.8 m above the gas sparger, using a conductance probe (Tacussel XE100) connected to a conductimeter and a computer.

The axial liquid dispersion coefficient E_{zl} was calculated by fitting the Inoue and Ohki [18] and Kafarov et al. [19] model to the experimental curve generated for the pulse response. Inoue and Ohki [18] and Kafarov et al. [19] have considered that the propagation process is described in analogy to Fick's Second Law

$$\frac{\partial C}{\partial t} = E_{zl}\frac{\partial^2 C}{\partial x^2}$$

solution of this equation gives

$$\frac{C(t,\mathrm{Z})}{C_\mathrm{o}} = 1 + 2\sum_{n=1}^{\infty}\left[\left(\cos n\pi\frac{Z}{L}\right)\exp\left(-\frac{n^2\pi^2}{L^2}E_{zl}t\right)\right]$$

Table 2
Column and sparger connection

Columns	Spargers	Turbulent bed	Inversed turbulent bed
1	Membrane I	X	X
	Perforated plate	X	X
2	Membrane II		X

Table 3
Physical properties of particles

Solid type	Diameter dp (mm)	Density ρ_s (kg/m^3)	Composition
PS1	4	1028	Polystyrene
P1	3.76	934	Polyethylene

in which Z is the distance between feed and measuring point, $x = Z/L$ is the dimensionless longitudinal co-ordinate and C_o represents the tracer concentration when $t = \infty$.

3. Results and discussion

3.1. G–L systems (BC)

On the basis of the previous results [6] we tried to define a general diagram for determining the gas flow conditions and the characteristics of the axial liquid mixing from a measurement of the dispersion coefficient E_{zl} only. This diagram (Fig. 3), uses the Peclet number versus the Froude number

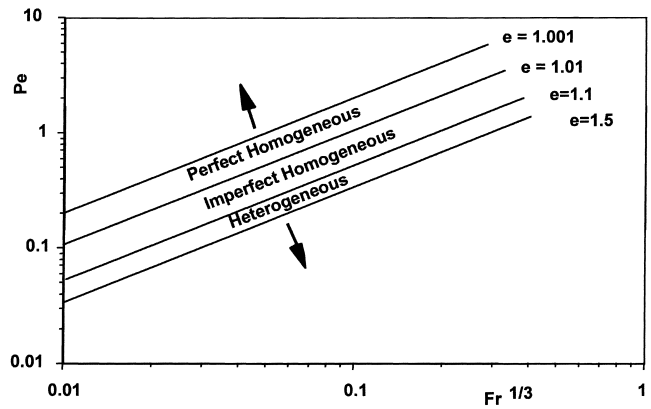

Fig. 3. General diagram Pe vs. $\mathrm{Fr}^{(1/3)}$.

Table 1
Gas sparger characteristics

Gas spargers	Sq. pitch arrangement (mm)	Orifice diameter (mm)	Holes (per cm^2)	Thickness (mm)
Perforated plate	5	2.5	4	20
Membrane I	5	(initial 0.5)	4	2.5
Membrane II	2.5	(initial 0.5)	16	2

Table 4
Initial weight of solids introduced into the G–L–S reactors

Columns	Spargers	Turbulent bed m_p (kg)	Inversed turbulent bed m_p (kg)
1	Membrane I Perforated plate	2–4–6–8–10–12–14–16–18–20–22	10–14–20–28–35
2	Membrane II		25–50–75–100–125

Table 5
Relation between gas flow regime and $Pe/Fr^{(1/3)}$

$Pe/Fr^{(1/3)}$	Gas flow regime	Gas sparger
2.5 to 5	Heterogeneous flow	Perforated plate membrane
5 to 10	Imperfect homogeneous flow	Perforated plate membrane
greater than 10	Perfect homogeneous flow	membrane

as co-ordinates for various values of the ratio $e = U_s/U_{b_\infty}$, which is known to influence the gas flow conditions.

For a given value of E_{zl}, at the given operating conditions, the Froude and Peclet numbers are easily deduced. The point (Pe, $Fr^{(1/3)}$) in the diagram, allows the value of e and the type of the gas flow to be found. In other words, the ratio $Pe/Fr^{(1/3)}$ gives information on the gas flow regime. From this general diagram one can define three ranges of variation of this ratio corresponding to different gas flow regimes. They are shown in Table 5. The established diagram was tested and validated against previous results in the literature.

Deckwer et al. [1] proposed the following relation established with a perforated plate as the gas sparger

$$E_{zl} = 0.678 D_c^{1.4} U_g^{0.3}$$

When this equation is used with various gas velocities up to 10 cm s^{-1}, the ratio $Pe/Fr^{(1/3)}$ ranges from 3 to 3.5, which is characteristic of the heterogeneous gas flow usually encountered with this type of gas distributor.

Rice et al. [4] characterized the axial liquid mixing in BCs of various diameters (5.08, 10.16, 15.24 and 30.48 cm), equipped with membrane and perforated plate spargers. They reported that the highest values of the coefficient E_{zl} were always reached with the perforated plate. The ratio $Pe/Fr^{(1/3)}$, computed from their data, were found to vary from 4.5 to 6 with the perforated plate and from 5 to 11.5 with the membrane. These results are in good agreement with the present analysis. It is worth noting that the membrane is the only sparger which can provide values greater than 10 for the ratio $Pe/Fr^{(1/3)}$. This is characteristic of a perfect homogeneous gas flow.

Kato et al. [10] measured the dispersion coefficient E_{zl} in BCs of different inner diameters (6.6, 12.2 and 21.4 cm) equipped with three types of perforated plate. They proposed an empirical relation to predict the Peclet number, defined as

$$Pe = \left(\frac{\eta_l}{\eta_w}\right)^{0.07} \left[\frac{13Fr^{0.5}}{1 + 6.5Fr^{0.4}}\right] \qquad (BC)$$

This relation was used to determine the ratio $Pe/Fr^{(1/3)}$ over the range of operating conditions (D_c, U_g) and was found to range from 2.5 to 3.1; these values express a heterogeneous type of gas flow which is indeed observed with this gas sparger.

It can be concluded that this general diagram, $Pe/Fr^{(1/3)}$ can be successfully tested over a wide range of operating conditions, and gives a good prediction of the nature of the gas flow and of the axial liquid mixing by measurement of the axial liquid dispersion coefficient E_{zl} only.

3.2. G–L–S systems

In G–L–S systems, the presence of a solid phase can change the liquid axial mixing. Therefore, the axial liquid mixing was characterized in two multiphase reactors: the turbulent bed and the inverse turbulent bed. In these G–L–S systems, the particles are fluidized by an upward gas flow. In the first, the solids are heavier than water; in the second, the particles are lighter than water.

3.2.1. Turbulent bed

In this reactor with no gas flow the bed of particles remains stationary at the bottom of the column, just above the gas sparger. The main difference between this reactor and the classical TPFB is that the minimum gas velocity U_{gc} required to fluidize the particles increases with the weight of solids introduced.

Axial liquid mixing experiments were performed for various values of mass number Ma over a range of superficial gas velocities above U_{gc}, i.e. when all the solid was in motion inside the column. The variations of E_{zl} with U_g for membrane and perforated plate spargers in column 1, are reported in Fig. 4(a) and Fig. 4(b), respectively, for different weights of solids m_p. Fig. 4(a) indicates that, with the membrane sparger, E_{zl} increases with increasing mass of solid. When the solid loading increases, the solid concentration near the membrane is important, aiding bubble coalescence and leading to an increase in bubble diameter and E_{zl}. On the contrary, with a perforated plate distributor

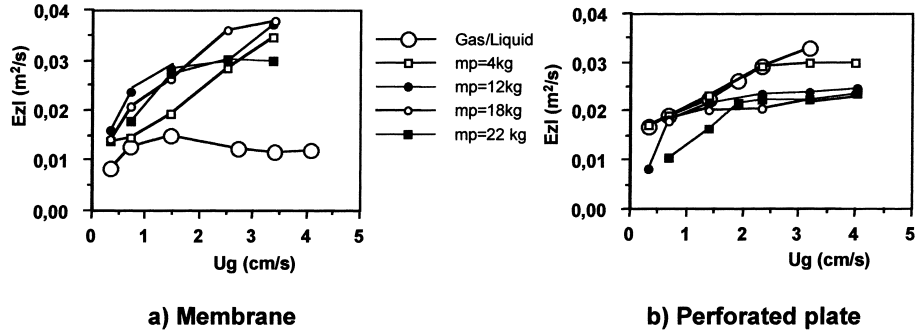

Fig. 4. Variations of E_{zl} with U_g-turbulent bed – column 1.

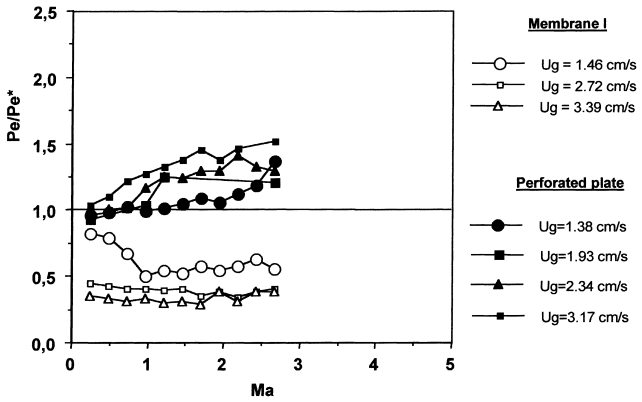

Fig. 5. Variation of the ratio Pe/Pe* with the mass number Ma.

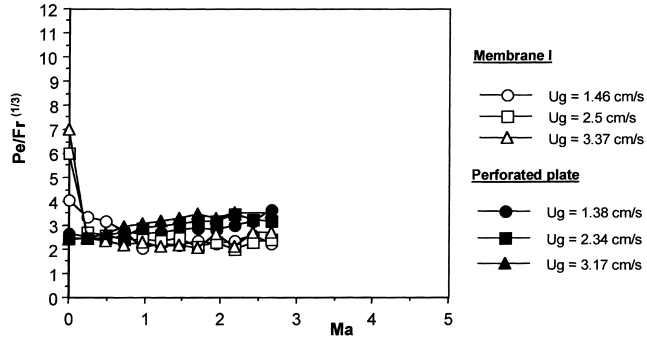

Fig. 6. $Pe/Fr^{(1/3)}$ vs. Ma in turbulent bed for membrane and perforated plate.

(Fig. 4(b)), E_{zl} decreases when the weight of solid increases. In this case, at the bottom of the column, the solids reduce the bubble distribution provided by the perforated plate, leading to a decrease in E_{zl}.

To compare the axial liquid mixing created by the membrane and the perforated plate in a turbulent bed, with and without solids, Fig. 5 shows the variations of the ratio Pe/Pe^* with the mass number Ma. Pe and Pe^* are the values estimated with and without solids, respectively. For the membrane, Fig. 5 shows that, whatever the superficial velocities and mass numbers, Pe/Pe^* is less than unity. The axial liquid mixing in a G–L–S reactor is greater than that in a G–L reactor at the same gas flow rate. In this case, the solids act as a local mixer. For the perforated plate, whatever the superficial velocities and mass numbers, Pe/Pe^* is greater than unity. This means that the axial liquid mixing in a G–L–S systems is lower than that in a G–L system. In this case, the particles act as a mixing inhibitor.

To characterize the effect of the gas sparger on the axial liquid mixing in a turbulent bed, Fig. 6 gives the variations of $Pe/Fr^{(1/3)}$ with the mass number Ma. By analogy with the general diagram $Pe = f(Fr^{(1/3)})$ defined previously for the G–L system, it can be seen in Fig. 6 that, whatever the gas sparger and mass number, the values of $Pe/Fr^{(1/3)}$ are around 3, which is characteristic of a heterogeneous gas flow. Moreover, Fig. 6 reveals that, in a turbulent bed, the gas sparger has very little effect on the axial liquid mixing. In fact, a lot of particles remain close to the bottom of the column, above the gas sparger. Then, even if the solids are in motion, this mass of particles acts as another gas sparger, inducing considerable liquid mixing.

To conclude it can be said that compared with G–L systems, in the turbulent bed reactor, the addition of particles can enhance or reduce the axial liquid mixing depending on the gas sparger used (membrane or perforated plate, respectively). However, irrespective of the gas sparger and the Mass number, the addition of particles in a G–L system modifies the intensity of the liquid mixing. From the general diagram $Pe/Fr^{(1/3)}$ extended to this G–L–S system, the addition of particles tends to lower the values of the ratio $Pe/Fr^{(1/3)}$, leading to large liquid circulations and heterogeneous gas flow.

3.2.2. Inverse turbulent bed

In this reactor, with no gas flow, the bed of particles remains stationary at the top of the column. Therefore, the effect of the gas sparger on the type of bubble distribution and on the liquid mixing can be expected to be more pronounced. Unlike in the turbulent bed, in this reactor the particles are easily distributed along the column, and the velocities required for the fluidization decrease as the weight of solids introduced into the system increases.

Axial liquid mixing experiments were performed with various values of the mass number Ma over a range of superficial gas velocities such that all the solid was in motion inside the column. The variations of E_{zl} with U_g

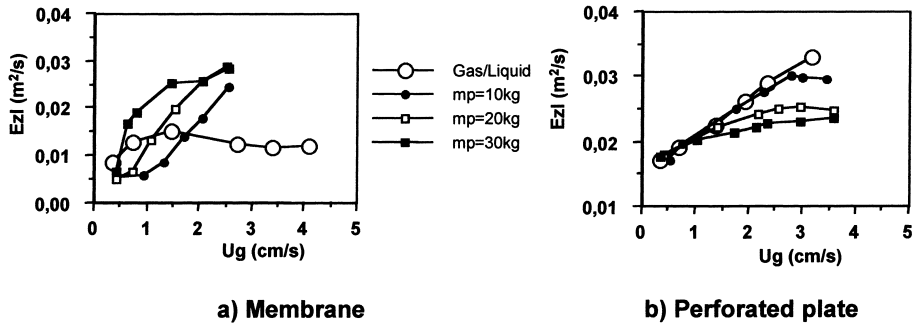

Fig. 7. Variations of E_{zl} vs. U_g = Inversed turbulent bed – column 1–2.

for different weights of solid m_p are shown in Fig. 7(a) indicates that, with the membrane sparger, the coefficient E_{zl} measured in inverse three-phase systems is higher than in a G–L reactor. The solids aid bubble coalescence when the membrane is used, leading to an increase in bubble diameter and E_{zl}. With the perforated plate (Fig. 7(b)), E_{zl} decreases when the weight of solid increases. In this case, the solids reduce bubble size distribution provided by the perforated plate and reduce E_{zl}. Different spargers give different trends of E_{zl} because they provide different bubble populations.

To compare the axial liquid mixing created by the membrane and perforated plate in an inverse turbulent bed, with and without solids, we give, in Fig. 8, the variations of the ratio Pe/Pe* with the non-dimensional number Ma. For the membrane Fig. 8 shows that, in the range of mass numbers Ma lower than 3, Pe obtained at $U_g = 1$ cm s^{-1} can be larger than Pe*. This means that the axial liquid mixing created in the G–L–S system is lower than that in the in G–L system, for the same gas throughput. Whatever the superficial gas velocity, if Ma > 3, Pe becomes lower than Pe*, and the axial liquid mixing created in the G–L–S system increases compared with that in the bubble column. As far as the inverse turbulent bed is concerned, when the membrane sparger is used, an increase in the mass number leads to a decrease in Pe/Pe*. For the perforated plate, the results are different irrespective of the gas velocity and mass number, Pe is always higher than Pe*. This means that the axial liquid mixing created in the G–L–S system is less than that in the

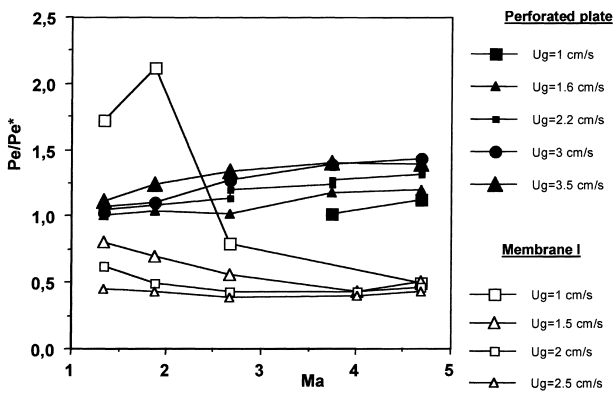

Fig. 8. Ratio Pe/Pe* vs. mass number Ma –inversed turbulent bed.

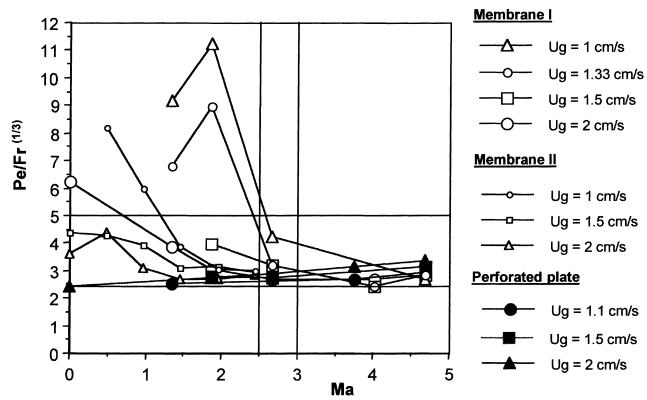

Fig. 9. Pe/Fr$^{(1/3)}$ vs. Ma in inversed turbulent bed for membrane I, Membrane II, and perforated plate.

G–L system. In this case, solids act as a mixing inhibitor. One can see that the ratio Pe/Pe* increases slowly with the mass number Ma. However, irrespective of the gas sparger and mass number, the addition of light particles to a G–L system modifies the liquid mixing.

To study the effect of the gas sparger on axial liquid mixing in an inverse turbulent bed, Fig. 9 shows the variations of Pe/Fr$^{(1/3)}$ for the membrane and perforated plate at different mass numbers Ma. By analogy with the general diagram Pe = f(Fr$^{(1/3)}$) defined previously for a G–L system, it can be seen in Fig. 9 that the experimental data are distributed in two ranges of values. The first interval, corresponding to Pe/Fr$^{(1/3)}$ values from 2.5 to 5, is characterized in the G–L system by a heterogeneous gas flow and a high level of liquid mixing. In this zone, we find all the experimental points obtained with the perforated plate and some points relative to the membrane sparger. The second interval, corresponding to Pe/Fr$^{(1/3)}$ values from 5 to 11, is characterized in the G–L system by an imperfect or perfect homogeneous flow and low axial liquid mixing. Only the experimental points obtained with the membrane spargers are to be found in this interval. It can be seen from Fig. 9 that, when the mass number Ma is larger than 3, the ratio Pe/Fr$^{(1/3)}$ reaches a constant value (2.5–3.5), independent of the sparger, characteristic of important axial mixing and heterogeneous gas flow. On the other hand, below Ma = 3, the Pe/Fr$^{(1/3)}$ values obtained with the membrane sparger are higher

than those obtained with a perforated plate, whatever the operating conditions. So in the range of mass numbers lower than 3, the ratio $Pe/Fr^{(1/3)}$ depends on the gas sparger used.

These results show that the gas flow conditions and, consequently, the liquid mixing are essentially affected by the gas sparger and the weight of solids when the mass number is less than 3. Beyond a critical value of solid concentration ($Ma > 3$), the gas sparger has no effect. In fact, in this case, the particles act on the gas flow as in a turbulent bed, inducing heterogeneous gas flow and enhancing liquid mixing.

To conclude, on the inverse turbulent bed it can be said that the liquid axial mixing can be affected by the mass number values and the gas sparger used. Moreover, large values of the ratio $Pe/Fr^{(1/3)}$ are only obtained in an inverse turbulent bed with a membrane sparger and a low mass number. The perforated plate leads to low values of this ratio in all operating conditions. So, it appears that the range of variation of $Pe/Fr^{(1/3)}$ is very large, i.e. the intensity of the liquid mixing depends strongly on the operating conditions (gas sparger, mass number).

3.2.3. *Comparison of axial liquid mixing in different multiphase reactors*

On the general diagram $Pe = f(Fr^{(1/3)})$, we have plotted the data obtained with our two G–L–S contactors, plus the data obtained by Kato et al. [20] with a classical three-phase fluidized bed.

Kato et al. [20] proposed the following relation by expanding the equation used earlier for liquid dispersion in the BC:

$$U_g < 9\,(\mathrm{cm\,s^{-1}}) \qquad Pe = \frac{U_g D_c}{E_{zl}} = \left(1 + \frac{U_t}{U_l}\right)^{0.4} Bo^{0.225}\, Pe \qquad (BC)$$

However, the drawback of this relation is that it does not take into account the gas sparger and the solid concentration.

The general diagram allows the hydrodynamic characteristics of one type of reactor to be compared with those of another, as shown in Fig. 10, where results obtained from three multiphase reactors are brought together. Fig. 10 shows that the axial liquid mixing created by an inverse turbulent bed equipped with a membrane, when $Ma < 3$ (open points), is lower than the mixing created by the other reactors (filled points) zone between the two straight lines corresponds to the data from Kato et al. [20].

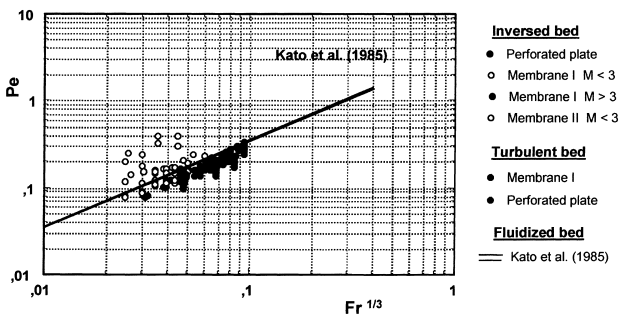

Fig. 10. General diagram used for three G–L–S contactors.

This result may be interesting for certain industrial application which require low axial liquid mixing. However, the Peclet number is not only a function of the Froude number; it also depends on the mass number and on the type of gas sparger used (Fig. 9). So, it would be better to propose a dimensionless number which takes into account the different characteristics of the gas sparger.

For all the other operating conditions (filled points and zone between the two straight lines), the ratio $Pe/Fr^{(1/3)}$ ranges from 2.5 to 4. These ratio values allow the Peclet number to be correctly predicted by the Froude number only in the three different tested reactors.

4. Conclusions

Axial liquid mixing was studied in G–L systems (bubble columns) and in two types of G–L–S system (turbulent and inverse turbulent bed).

In two-phase systems, the type of gas sparger has a strong effect on the gas flow regime and consequently on the axial liquid mixing. A general diagram with co-ordinates Pe versus $Fr^{(1/3)}$ has been established in order to explain all the results. It allows the hydrodynamic characteristics to be predicted by a simple measurement of the axial liquid dispersion coefficient.

In the G–L–S reactors tested (turbulent and inverse turbulent bed contactors), the effect of the gas sparger is less pronounced in the turbulent bed than in the inverse turbulent bed. Moreover, beyond $Ma = 3$, $Pe/Fr^{(1/3)}$ values are around 3, characterizing a heterogeneous gas flow regime, irrespective of the gas sparger and multiphase reactor used. These ratio values allow the Peclet number to be correctly predicted by the Froude number only, in the three different tested reactors.

The extension to these G–L–S reactors of the general diagram of Pe versus $Fr^{(1/3)}$ established for the G–L systems seems to be interesting, since it allows the hydrodynamic conditions to be predicted and the various reactors to be compared as far as these properties are concerned.

Appendix

Nomenclature

C_L	tracer concentration in the liquid phase ($mol\,l^{-1}$)
C_o	tracer concentration when $t = \infty$
D_c	column diameter (m)
d_p	particle diameter (m)
E_{zl}	axial liquid dispersion coefficient ($m^2\,s^{-1}$)
g	acceleration due to gravity ($m^2\,s^{-1}$)
m_p	weight of solids (kg)

$U_{b\infty}$ terminal velocity of air bubble (m s^{-1})
U_g superficial gas velocity (m s^{-1})
U_l superficial liquid velocity (m s^{-1})
U_s slip velocity (m s^{-1})
U_t terminal velocity of solid particle (m s^{-1})
V_c circulation velocity (m s^{-1})
V_s hindered settling velocity (m s^{-1})
x longitudinal co-ordinate (m)
Z distance (measuring point to feed point) (m)

Dimensionless numbers

Fr Froude number (U_g^2/gD_c)
Pe G–L–S Peclet number (U_gD_c/E_{zl})
Pe^* G–L Peclet number (U_gD_c/E_{zl})
Ma Mass number, ($m_p/(\rho_s D_c^3)$)
Bo Bond number ($gd_p^2\rho_l/\sigma$)

Greek symbols

ε_g fractional gas hold-up
ε_l fractional liquid hold-up
ε_s fractional hold-up of solids
ρ_l liquid density (kg m^{-3})
ρ_s solid density (kg m^{-3})
η_g viscosity of gas (Pa s^{-1})
η_l viscosity of liquid (Pa s^{-1})
η_w viscosity of water (Pa s^{-1})

References

[1] W.D. Deckwer, R. Burckhart, G. Zoll, Mixing and mass transfer in tall bubble columns, Chem. Eng. Sci. 29 (1974) 2177–2188.
[2] M.H.I. Baird, R.G. Rice, Axial dispersion in large unbaffled columns, Chem. Eng. J. 9 (1975) 171–174.
[3] J.B. Joshi, Axial mixing in multiphase contactors: a unified correlation, TransI ChemE 58 (1980) 155–165.
[4] R.G. Rice, J.M.I. Tupperainen, R.M. Hedge, Dispersion and holdup in bubble columns comparison of rigid and flexible spargers, Can. J. Chem. Eng. 59 (1981) 677–687.
[5] Y. Kawase, Moo- Young, Mathematical models for design of bioreactors: applications of Kolmogoroff's theory of isotropic turbulence, Chem. Eng. J. 43 (1990) B19–B41.
[6] G. Hébrard, D. Bastoul, M. Roustan, Influence of the gas sparger on the hydrodynamic behaviour of bubble columns, TransI ChemE, vol. 74, Part A, April 1996, 406–414.
[7] J.R. Grace, Shapes and velocities of bubbles rising in infinite liquids, TransI ChemE. 51 (1973) 116–120.
[8] G.B. Wallis, in: P.A. Rottenburg (Ed.), Interaction between fluids and particles, Int. Chem. Eng., 1962, p. 9.
[9] S. Nacef, G. Wild, A. Laurent, S.D. Kim, Scale effects in gas-liquid-solid fluidisation, Int. Chem. Eng. 32 (1992) 51–72.
[10] Y. Kato, A. Nishiwaki, T. Fukuda, S. Tanaka, The behaviour of suspended solid particles and liquid in bubble columns, J. Chem. Eng. Japan 5(2) (1972) 112–118.
[11] M.L. Michelson, K. Østergaard, Holdup and fluid mixing in gas-liquid fluidised beds, Chem. Eng. J. 1 (1970) 37.
[12] K. Østergaard, Holdup, mass transfer and mixing in the three-phase fluidisation, AIChE Symp. Ser. 74(176) (1978) 82.
[13] S.A. El-Temtamy, Y.O. El-Sharnoubi, M.M. El-Halwagi, Liquid dispersion in gas-liquid fluidised beds Part I, Chem. Eng. J. 18 (1979) 151–159.
[14] S.D. Kim, C.H. Kim, Axial dispersion characteristics of three phase fluidised beds, J. Chem. Eng. Japan 16(3) (1983) 172–178.
[15] P.B. Whalley, J.F. Davidson, Liquid circulation in bubble columns, in: Proc. Symp. Multiphase Flow Systems, Symposium Ser. No. 38.J.5, IChemE, London, 1974.
[16] M. Roustan, C. Beck, B. Capdeville, D. Bastoul, J.M. Audic, Hydrodynamic study of a multiphase reactor: the turbulent bed., Fluidisation VIII, Int. Symp. of the Engineering Foundation, vol 1, pp. 38, Tours, France, 1995.
[17] M. Roustan, G. Hébrard, M.P. Comte, C. Beck, D. Bastoul, J.M. Audic, Etude hydrodynamique d'un réacteur à lit fluidisé inversé., Récents progrès en génie des procédés, Lavoisier, vol. 9, 42, 1995, 81–86.
[18] H. Inoue, Y. Ohki, Longitudinal mixing of the liquid phase in bubble columns, Chem. Eng. Sci. 25 (1970) 1.
[19] V.V. Kafarov, V.G. Vygon, V.A. Rudakov, G.A. Mikheeva, Method for determining the coefficient of longitudinal mixing for the continuous phase under the conditions of a nonflow-through system in high-rate extractors, Teoreticheskie Osnovy Khimicheskoi Tekhnologii 7 4 (1973) 550–556 (translated).
[20] Y. Kato, A. Nishiwaki, T. Fukuda, S. Tanaka, The behaviour of suspended solid particles and liquid in bubble columns, J. Chem. Eng. Japan 18(4) (1985) 113–318.